Magnetic Resonance in Medicine 45:562–567 (2001)

Myocardial Wall Tagging With Undersampled Projection Reconstruction

Dana C. Peters,* Frederick H. Epstein, and Elliot R. McVeigh

Azimuthally undersampled projection reconstruction (PR) acquisition is investigated for use in myocardial wall tagging with MR using grid tags to provide increased temporal and spatial resolution. PR can provide the high-resolution images required for tagging with very few projections, at the expense of artifact. Insight is provided into the PR undersampling artifact, in the context of measuring myocardial motion with tags. For Fourier transform imaging, at least 112 phase-encodings must be collected to image tagging grids spaced 7 pixels apart. PR requires about 80 projections, a 1.4-fold reduction in scan time. Magn Reson Med 45:562–567, 2001. Published 2001 Wiley-Liss, Inc.†

Key words: tagging; projection reconstruction; myocardial wall motion; undersampling; radial imaging

Myocardial wall motion imaging is an important diagnostic tool for assessment of cardiac function (1). The constraint of breath-holding and the need for adequate temporal resolution limit the spatial resolution achievable for tagged imaging of the heart. Projection reconstruction (PR) imaging with a limited number of angles has a low artifact level with spatial resolution that is roughly independent of the number of projections (N_p) acquired (2). The image resolution is primarily determined by the readout resolution.

Here we investigate the ability of limited-angle PR to image myocardial wall motion with higher spatial and temporal resolution compared to Fourier transform imaging (i.e., raw data collected on a Cartesian grid, denoted here as FT). PR is investigated and compared to imaging with FT for tagging studies with grid patterns. Grid tags oriented at 45° with respect to the readout direction were chosen because they yield a 2D displacement field in a single acquisition.

For imaging grid patterns oriented at 45° to the readout direction, FT imaging faces the challenge of achieving adequate spatial resolution in both the *x* and *y* directions without a long breath-hold or a long temporal window within the cardiac cycle. Increasing the temporal window results in motion blurring, and increased breath-holds are not well tolerated by patients. To achieve adequate temporal and spatial resolution during a breath-hold, investigators have used echo-planar trajectories (3–5). One of the most efficient *k*-space reduction methods (6,7) uses stripe tag patterns, and acquires a narrow band of central *k*-space with good resolution only in the frequency-encoding direction. This adequately samples the tags, which are oriented perpendicular to the frequency-encoding direction, but requires that the frequency-encoding direction be swapped to obtain two orthogonal sets of tags, leading to potential aliasing. Grid tag imaging of the heart with 7-pixel spacing has been reported using a 256 readout resolution and from 144 (8) to 128 phase-encodings (9–11).

The purpose of this investigation is to determine the number of views, either phase-encodings or projections, required to image grid tags using FT and projection reconstruction. The number of views was reduced in the FT acquisition by collecting fewer phase-encodings, i.e., lower resolution in the y direction. The number of views was reduced in the PR acquisition by collecting fewer projections, i.e., high spatial frequency aliasing.

The reduction in the number of projections in PR results in a lower signal-to-noise ratio (SNR) due to decreased averaging and to artifact that appears as either noise or streaks. The artifact due to a limited number of projections is dependent on the anatomical configuration to be imaged, which is predictable in the heart. Figure 1 shows a short-axis view of the heart reconstructed with a 256 readout resolution and 256, 128, 64, and 32 projections. Even at 32 projections the endo- and epicardial borders are well delineated.

These good results and the results of others (12) suggest that PR can obtain *tagged* images of the heart with very few projections, while providing 256 × 256 resolution, and good temporal and spatial resolution. Here we investigate the ability of limited-angle PR to image tags with fewer views than is required for FT imaging.

THEORY

When the tag pattern is applied to the spin magnetization in the object, this creates distinct peaks in *k*-space. The tag pattern can be represented as a comb function in image space, with spacing Tagspc. The positions of *k*-space peaks are related to the tag pattern by:

$$S(k)_{tag} = FT\left[\, comb\left(\frac{x}{Tagspc}\right)\right] = comb\left(\frac{k}{1/Tagspc}\right). \quad [1]$$

Figure 2 shows grid tags on the heart wall and its *k*-space representation. The tags were spaced 7 pixels apart in the image, with 256 frequency- and phase-encodings. The *k*-space representation shows a central peak and peaks at positions labeled $(k_r, k_\theta) = (\pm 0.14, 45°$ and $135°)$, $(\pm 0.28, 45°$ and $135°)$, etc., corresponding to multiples of $(1/7 = 0.14)$ of *k*-space, where *k*-space is normalized to extend from ±0.5. The *k*-space peaks are also labeled in pixel

Laboratory of Cardiac Energetics, National Institutes of Health, Bethesda, Maryland.

*Correspondence to: Dana C. Peters, National Institutes of Health, 10 Center Drive, Bldg. 10 B1D416, Bethesda, MD 20892-1061. E-mail: petersd@nih.gov

Received 20 October 2000; revised 18 December 2000; accepted 9 January 2001.

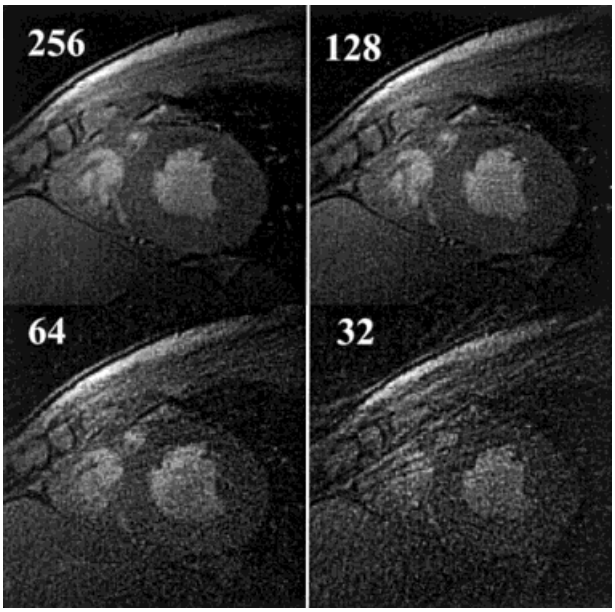

FIG. 1. A short-axis slice of the heart with 256 × 256 in-plane resolution, reconstructed with 256, 128, 64, and 32 projections. This demonstrates that undersampled PR is well suited for cardiac imaging. Notice that the endocardial border is well resolved, even with 32 projections.

coordinates (k_x, k_y) in Fig. 2, normalized to ± 128. Note that there are off-diagonal peaks (one is circled in Fig. 2). These arise from convolving the two orthogonal tag patterns. They represent the tag intersecting points in the image, and are significant to accurate tag imaging (13). In this work we obtain the lower limit on the number of views required for imaging this type of tag pattern in the heart. Both the PR and FT acquisitions must adequately sample the tagging signal located at the peaks shown in Fig. 2.

Sampling for FT

The two influences on tag position estimation accuracy are image noise, and the tag pattern shape (14). Delineation of tag pattern shape depends on sampling the *k*-space peaks of the tag pattern, as shown in Fig. 2. This requires high spatial resolution in the *x* and *y* directions. The tags can are delineated by these peaks, which occur at $k_r = \pm 1/7$, 2/7, and 3/7 cycles/pixel (for 7-pixel spacing, as in Fig. 2). In terms of phase-encoding lines, the first peaks corresponds to $2 \cdot (1/7) \cdot \cos(45°) \cdot 256 = 51.5$ phase-encodings. The second and third peaks can be captured by acquiring more than 103 and 155 phase-encodings, respectively.

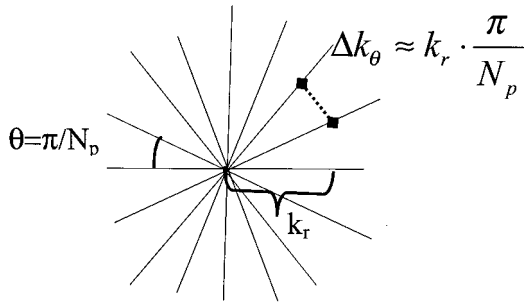

FIG. 3. Sampling scheme for undersampled PR. The FOV for each frequency (k_r,θ) in *k*-space is determined by the azimuthal spacing Δk_θ (k_r).

Sampling for PR

For PR, decreased numbers of projections provide maintained resolution, reduced scan time, lower SNR, and increased artifacts. The image produced by angular undersampling can be obtained by convolving the angularly undersampled point spread function (PSF) with the artifact-free image. The PSF provides insight into the artifact from undersampling; however, additional insight can be obtained using the concept of wraparound artifact or aliasing caused by undersampling. The outcome of undersampling *k*-space at the specific frequencies of the tags (see Fig. 2) must be determined. The outcome of undersampling has been previously investigated for x-ray CT (15–17) and for MR (2,18); however, nothing comparable to the Nyquist theorem of FT imaging exists for PR.

We present here a discussion of the artifact generated by azimuthal undersampling of each spatial frequency. The projections are obtained at evenly spaced angles. The sampling of *k*-space along projections is shown in Fig. 3. The undersampling increases linearly with k_r. The FOV for a signal at a position in *k*-space (k_r, θ), FOV(k_r), is determined by the azimuthal spacing of samples, Δk_θ (k_r), in analogy to the FOV in Cartesian sampling:

$$\frac{1}{FOV(k_r)} = \Delta k_\theta(r) \approx \frac{\pi}{N_p} \cdot k_r. \qquad [2]$$

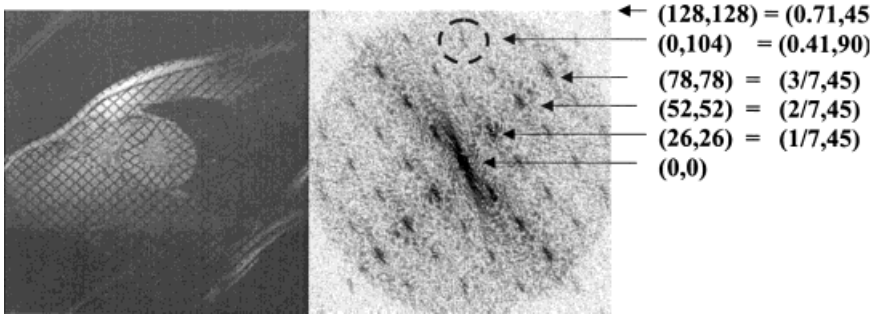

FIG. 2. Example of a tagged image of the heart, using grid tags oriented at 45°. The *k*-space representation shows strong peaks throughout the k_x-k_y plane. Sampling and representing the tags requires high spatial resolution in the *x* and *y* directions. The positions of the peaks determine the extent of the k_y data that must be acquired. The positions of the spectral peaks are labeled using polar coordinates (k_r,θ) with k_r normalized to ±0.5, and in (k_x,k_y) coordinates normalized to ±128.

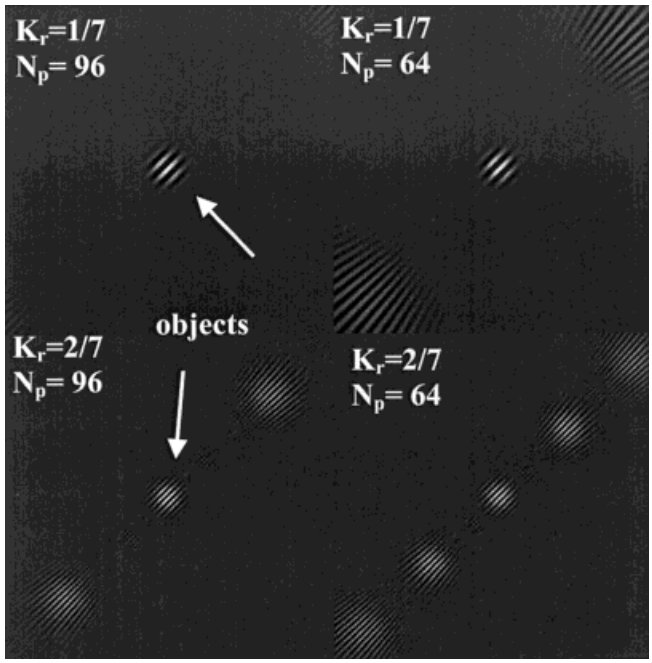

FIG. 4. A central Gaussian 9 pixels in width, multiplied by a plane wave of a discrete spatial frequency, is subject to undersampling. The artifact pattern is shown for 96 and 64 projections, and carrier frequencies of k_r =1/7 and 2/7. The artifact generated by the localized plane waves appears at a distance predicted by Eq. [2]. The signal intensity and frequency of the artifacts are about the same as the signal and frequency of the generating object. See Table 1.

Simulations demonstrate how the aliasing appears in the image. A plane wave in image space, with frequency k_r, oriented at a 45° angle, was generated, and multiplied with a central Gaussian 9 pixels in width. This represents a 2D wave packet, a central localized signal of a particular frequency. This image was subject to undersampling, to observe the aliasing pattern. Figure 4 shows the undersampled objects with carrier frequencies k_r = 1/7 and 2/7 cycles/pixel. These frequencies were chosen because they represent the tag frequencies. The undersampled images were reconstructed with 64 and 96 projections. The images show the centrally located original object and the artifact. The artifact appears as signal at the original frequency replicated at a distance from the original object, which is determined by Eq. [2]. Note that increasing the number of projections moves the artifact away from the object. The artifact appears as a signal of about the same intensity and frequency as the object that produced it, at a predictable distance from the orignal object. The artifact is characterized in Table 1. The distance between the aliasing and the central artifact-generating object is compared to the predicted distance. The ratios of the aliasing signal to the original signal are compared, and the wavelength of the aliasing modulation is compared to the original wavelength. Figure 6 and Table 1 support the view that aliasing of a particular spatial frequency appears at an FOV given by Eq. [2], with a frequency and signal comparable to the original signal and frequency. If the object shifts within the FOV, the artifact pattern shifts accordingly.

With these considerations, undersampling of the tag frequencies is limited by the requirement that aliasing of tag frequencies should not obscure the object of interest, i.e., that aliasing from one tagged object should not overlie the tagged myocardium.

Reduction in numbers of projections (N_p) also results in reduced SNR, through a well-known dependence on averaging, $SNR \propto \sqrt{N_p}$. However, signal collection efficiency ($SNR/\sqrt{N_p}$) is maintained until, at low N_p, undersampling produces artifact that acts as noise to obscure the image.

METHODS

Data Acquisition and Reconstruction

The 2D PR pulse sequence and the PR trajectory are described in Ref. 2. The pulse sequence was a modification of a commercial ECG-gated 2D fast segmented multiphase gradient-echo sequence with tagging preparation pulses. All of the projections were divided into N angular regions, with N equal to the number of views per segment. The timing of the segmented acquisition is such that all of the projections in an angular region were collected at the same delay time with respect to the start of each cardiac phase.

The sequence was implemented on a GE 1.5 Tesla LX scanner equipped with 4 G/cm gradient strengths and slew rates up to 120 mT/m/s. A cardiac phased-array coil was

Table 1
The Artifacts of Figure 4 Are Characterized by Their Wavelength, Distance From the Original Object, and Signal Intensity of Artifact Relative to the Original Object, Using Numbers of Projections, N_p = 64 and 96, and Central Wave Packet Spatial Frequencies k_r = 1/7 and 2/7 Cycles/Pixel

K_r, N_p	Wavelength of central wave packet (pixels)	Wavelength of artifact (pixels)	Distance between central wave packet and artifact	Predicted distance (pixels)	Artifact signal (peak to peak) ÷ wave packet signal
K_r = 1/7 N_p = 64	7	~7	~144	142.6	63%
K_r = 2/7 N_p = 64	3.5	~3.5	~72	71.3	88%
K_r = 1/7 N_p = 96	7	Not observed	>181	213.8	Not observed
K_r = 2/7 N_p = 96	3.5	~3.5	~109	106.9	58%

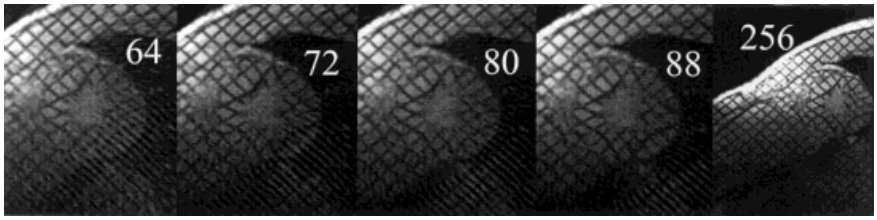

FIG. 5. The results of convolving undersampled PSFs for 64, 72, 80, and 88 projections with a fully sampled tagged image. A view of the entire FOV reconstructed with 256 projections is also shown. Visual inspection shows that the undersampling artifact arises mainly from the hyperintense signal on the anterior chest wall. The artifact recedes from the myocardium as more views are used.

used for human volunteers. The grid pattern was applied with presaturation pulses consisting of seven tagging SPAtial Modulation of Magnetization (SPAMM) RF pulses (19) with relative amplitudes (5,7,9,10), oriented at 45° from the readout direction and spaced 7 pixels apart, with a composite 180° flip angle. The reconstruction of data was performed offline using a regridding algorithm (20) and 2D FT of the data.

Simulations

In order to predict the result of acquiring images of the heart with reduced numbers of projections, fully sampled tagged magnitude MR images ($I(x,y)$) of the heart were obtained, and convolved with the well known undersampled PR PSF with reduced numbers of projections (18) to obtain an image with artifact, $\hat{I}(x,y)$: $\hat{I} = PSF\ (Np) \otimes I(x, y)$. The input MR image was acquired with scan parameters: 36-cm FOV, 8-mm slice, full echo, TR/TE/flip = 7.0ms/2.0ms/12°, ± 32 kHz BW, grid tags spaced at 7 pixels, oriented at 45°, 256 × 256 projections, cardiac phased-array coil. It was necessary to use a human tagged cardiac image for this simulation to determine the conditions under which the artifact from tagged objects in the FOV overlies the heart. Convolution with a PSF has an advantage over reconstructing a fully sampled image with reduced number of views, because the outcome of using an arbitrary number of projections can be simulated from the same data.

Imaging Experiments

Phantom experiments were performed with a circular uniform water and copper sulfate phantom. PR and FT acquisitions were obtained with grid tag patterns at 45°. Internal Review Board approved informed consent was obtained from all volunteers. In normal volunteers, single mid-ventricular short-axis slices were imaged using PR and FT acquisitions with equal numbers of views. A 256 readout resolution, and 64–256 phase-encodings or projections were acquired, and the PR and FT images were compared.

RESULTS

Simulations

Figure 5 shows the result of convolving a tagged, fully sampled short-axis image of the myocardium with undersampled PSFs. Visual inspection shows that the tagged hyperintense anterior chest wall is generating the artifact, which appears on the posterior free wall of the myocardium. The artifact moves steadily away from the wall as the number of projections is increased. Using Eq. [2], the predicted distance between the the anterior chest wall and the artifact it generates (due to the signal at k_r = 2/7 cycles/pixel) is 71, 80, 89, and 98 pixels, which agrees roughly with measurements on the images in Fig. 5. The simulation indicates that between 64 and 96 projections, acceptable undersampled images can be obtained for this geometry.

Phantom Experiments

Tagged phantom images using 256, 168, 144, 112, 96, and 64 views are shown in Fig. 6. Qualitatively, reduced views provide images of lower SNR, appreciable artifact, and resolution equal to fully sampled images for PR. For FT, tag sharpness decreases, but SNR improves. The FT grid pattern's sharpness decreases suddenly between 168 and 144 phase-encodings because of the loss of the third *k*-space peak (see Fig. 2). Between 112 and 96 lines, the FT tags drastically deteriorate because of the loss of the second *k*-space peak (see Fig. 2). These phantom results suggest that low-resolution tagging studies should acquire *k*-space data just beyond one of these transition points. In particular, the tag pattern can be delineated with two harmonics, or by sampling just beyond k_r = ± 2/7 cycles/pixel (for 7-pixel spacing). This corresponds to acquiring more than 103 phase-encodings (see Fig. 2).

In Vivo Experiments

Figure 7 compares tagged images of the heart in a human volunteer for FT and PR. The tagged myocardium image

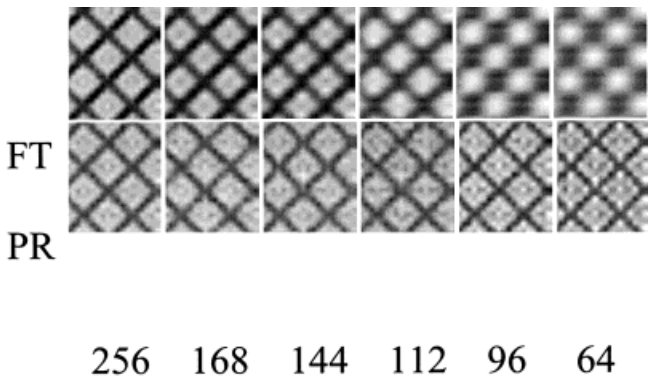

FIG. 6. Tagged phantom images using 256, 168, 144, 112, 96, and 64 views. Top row: FT grids; bottom row: PR grids.

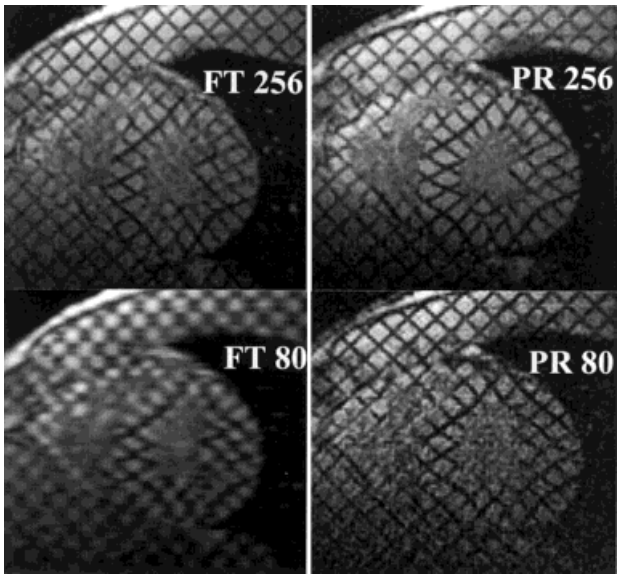

FIG. 7. Tagged images of the heart using PR and FT. With 80 projections, PR provides superior tag delineation in a scan time equal to that of FT.

was acquired with an 80 projection PR acquisition, and an 80 phase-encoding FT acquisition. The scan parameters were: 32-cm FOV, 256 readout resolution, grid-tags spaced 7 pixels apart oriented at 45°, eight views per segment, 8-mm-thick slice, TR/TE/flip = 7.1 ms/2.1ms/10°, ±32 kHz BW, full echo, 10-heart-beat breath-hold.

The PR image provides clearer tag delineation than FT, with 80 views. Corresponding FT and PR images obtained with 256 views are also shown.

DISCUSSION

This investigation shows that FT imaging of tags requires at least 112 phase-encodings to track the tags for grids oriented at 45°, spaced 7 pixels apart. This limit varies inversely with tag spacing. If fewer than 112 phase-encodings are obtained, tag line contrast is very low (see Figs. 6 and 7), so this is a strong lower limit. One hundred-sixty phase-encodings will improve tag line delineation further (third harmonic in Fig. 2). Additional phase-encodings will only increase scan time, and reduce SNR, and will not provide better tagged images.

For PR imaging, about 80 projections are required to image tags spaced 7 pixels apart. This limit also scales inversely with tag spacing. This represents a speed increase of about 1.4 compared to FT imaging. Eighty projections provide an FOV of about 89 pixels for the tag signal from the second harmonic in *k*-space. This moves the artifact from the anterior chest wall away from the myocardium (see Fig. 5). This number will vary some from person to person, and with FOV.

This investigation determined the minimum sampling requirements in terms of phase-encodings and projections for tagged imaging. However, other methods can be used to provide further reductions in the actual number of views acquired. Reduced FOV imaging can be implemented in conjunction with multiphase imaging for FT (21) or PR (18,22), providing the opportunity to reduce the scan time, or obtain reduced artifact for PR, and increased resolution for FT. Although many published tagging studies employed full FOVs, fractional FOV (3/4 FOV) can be used with FT techniques to provide higher resolution without increase in scan time. The undersampled PR images already enjoy the benefits associated with a partially empty FOV because less material is available for aliasing. The undersampling techniques SENSitivity Encoding (SENSE) (23) and Simultaneous Acquisition of Spatial Harmonics (SMASH) (24) may be applied to either method, offering additional reductions in speed, although to date they have not been used for PR.

This study compares the ability of PR and FT to spatially resolve grid tags using reduced numbers of views, focusing on the tradeoffs between the low resolution of FT, and the artifacts of PR. The SNR is often the critical factor in establishing an imaging protocol. The imaging protocol used in this study provided adequate SNR for each method. However, if thinner slices, higher bandwidths, or smaller FOVs were chosen, the SNR reductions would reduce the PR image quality more than FT, because of the already low SNR of the undersampled high-resolution PR images. In order to obtain acceptable images with undersampled PR, imaging protocols with increased SNR are needed. Potential methods for improving SNR include true fast imaging with steady state precession (FISP) imaging, lower bandwidth imaging, and improved coils. SNR can be increased for cardiac cine imaging by increasing the effective TR through slice interleaving (25).

The imaging of tagged myocardium presents the greatest challenge for undersampled PR, which relies on the limited signal strength of high spatial frequencies. Although images of left ventricular function can be adequately sampled with as few as 32 projections (Fig. 1), the intentional introduction of sharp tag lines for tracking the discrete material points of the myocardium provides increased signal strength at specific high spatial frequencies, creating artifact. Figure 4 and Table 1 provide insight about the generation of artifacts by undersampling for specific frequencies. The undersampled signal at a specific frequency appears in the image at its proper location, and in another location displaced by its alias-free FOV(k_r) with a similar signal strength and frequency. The lower spatial frequencies do not alias at all. For purposes of tagging, the ability to predict the position, relative to a tagged object, of the aliasing of the tag frequencies is useful. For tags, the artifacts are acceptable if the number of projections is great enough to displace them from the object of interest, the myocardium.

CONCLUSIONS

This investigation finds that PR requires fewer views than FT for imaging grid tags oriented at 45°. For FT imaging, at least 112 phase-encodings are needed to image grid tags with 7-pixel spacing. For PR imaging, reduced numbers of projections are acceptable until the artifact from the anterior chest wall appears on the myocardial wall, which occurs at about $N_p = 80$. SNR also limits the reduction in numbers of projections. PR can provide a scan-time reduction of 1.4 compared to FT.

REFERENCES

1. McVeigh ER. Regional myocardial function. Card Clinics 1998;16:189–206.
2. Peters DC, Korosec FR, Grist TM, WF Block, Vigen KK, Holden JE, Mistretta CA. Undersampled projection reconstruction applied to MR angiography. Magn Reson Med 2000;43:91–101.
3. Reeder SB, Atalar E, Faranesh AZ, McVeigh ER. Multi-echo segmented k-space imaging: an optimized hybrid sequence for ultra-fast cardiac imaging. Magn Reson Med 1999;41:375–385.
4. Stuber M, Fischer SE, Sheidegger MB, Boesiger P. Toward high-resolution myocardial tagging. Magn Reson Med 1999;41:639–643.
5. Epstein FH, Guttman MA, McVeigh ER, Myocardial tagging at frames exceeding 100 frames per second. In: Proceedings of the 8th Annual Meeting of ISMRM, Denver, 2000. p 1609.
6. Fischer SE, McKinnon GC, Maier SE, Boesiger P. Improved myocardial tagging contrast. Magn Reson Med 1993;30:191–200.
7. McVeigh ER, Atalar E. Cardiac tagging with breath-hold cine MRI. Magn Reson Med 1992;28:318–327.
8. Marcus JT, Gotte MJW, Van Rossum AC, Kuijer JPA, Heethaar RM, Axel L, Visser CA. Myocardial function in infracted and remote regions early after infarction in man: assessment by magnetic resonance tagging and strain analysis. Magn Reson Med 1997;38:803–810.
9. Geskin G, Cramer CM, Rogers WJ, Theobald TM, Pakstis D, Hu Y-L, Reichek N. Quantitative assessment of myocardial viability after infarction by dobutamine magnetic resonance tagging. Circulation 1998;98:217–233.
10. Young AA, Imai H, Chang CN, Axel L. Two-dimensional left ventricular deformation during systole using magnetic resonance imaging with spatial modulation of magnetization. Circulation 1994;89:740–752.
11. Kramer CM, McCreery CJ, Semonik L, Rogers WJ, Power TP, Shaffer A, Reichek N. Global alterations in mechanical function in healed reperfused first anterior myocardial infarction. J Cardiovasc Magn Reson 2000;2:33–41.
12. Barger AV, Grist TM, Block WF, Mistretta CA. Single breath-hold 3D multiphase contrast-enhanced method for assessment of cardiac function. Magn Reson Med 2000;44:821–824.
13. Doyle M, Walsh EG, Foster RE, Pohost GM. Common k-space acquisition: a method to improve myocardial grid-tag contrast. Magn Reson Med 1997;37:754–763.
14. Atalar E, McVeigh ER. Optimization of tag thickness for measuring position with magnetic resonance imaging. IEEE Trans Med Imaging 1994;13:152–160.
15. Smith PR, Peters TM, Bates RHT. Image reconstruction from finite numbers of projections. J Phys A: Math Nucl Gen 1973;6:361–382.
16. Joseph PM. View sampling requirements in fan beam computed tomography. Med Phys 1980;7:692–702.
17. Glover GH, Eisner RL. Theoretical resolution of computed tomography systems. JCAT 1979;3:85–91.
18. Scheffler K, Hennig J. Reduced circular field-of-view imaging. Magn Reson Med 1998;40:474–480.
19. Axel L, Dougherty L. MR imaging of motion with spatial modulation of magnetization. Radiology 1989;171:841–845.
20. Jackson JI, Meyer CH, Nishimura DG. Selection of a convolution function for Fourier inversion using gridding. IEEE Trans Med Imaging 1991;10:473–478.
21. Madore B, Glover G, Pelc N. Unaliasing by Fourier-encoding the overlaps using the temporal dimension (UNFOLD) applied to cardiac imaging and fMRI. Magn Reson Med 1999;42:813–828.
22. Weiss S, Rasche V. Projection-reconstruction reduced FOV imaging. Magn Reson Imaging 1999;17:517–525.
23. Pruessmann KP, Weiger M, Scheidegger MB, Boesiger P. Sense: sensitivity encoding for fast MRI. Magn Reson Med 1999;42:952–962.
24. Sodickson DK, Griswold MA, Jakob PM, Edelman RR, Manning WJ. Signal-to-noise ratio and signal-to-noise efficiency in SMASH imaging. Magn Reson Med 1999;41:1009–1022.
25. Herzka DA, Epstein FH, McVeigh ER. Improved SNR in breath-hold cardiac cine imaging by slice interleaving. In: Proceedings of the 8th Annual Meeting of ISMRM, Denver, 2000. p 1529.